Dalton Transactions

Long-Range Coupling in Cyclic Silanes

Journal:	*Dalton Transactions*
Manuscript ID	DT-ART-09-2020-003163.R1
Article Type:	Paper
Date Submitted by the Author:	15-Oct-2020
Complete List of Authors:	Ferguson, John; Johns Hopkins University - Homewood Campus Jiang, Qifeng; Johns Hopkins University - Homewood Campus Marro, Eric; Johns Hopkins University - Homewood Campus Siegler, Maxime; Johns Hopkins University, Chemistry Klausen, Rebekka; Johns Hopkins University, Chemistry

ARTICLE

Long-Range Coupling in Cyclic Silanes

John T. Ferguson,[a] Qifeng Jiang,[a] Eric A. Marro,[a†] Maxime A. Siegler,[a] Rebekka S. Klausen*[a]

Received 00th January 20xx,
Accepted 00th January 20xx

DOI: 10.1039/x0xx00000x

We report the synthesis of a mixed methyl- and hydro-substituted cyclosilane (**1**) possessing cis/trans stereoisomerism. Each diastereomer of **1** possesses distinct symmetry elements (*cis*-**1**: C_s-symmetric; *trans*-**1**: C_2-symmetric). Cyclosilane **1** is a model system to probe configuration- and conformation-dependent long-range proton-proton coupling. Extensive NMR spectroscopic characterization is reported, including one-dimensional ^{1}H NMR and ^{29}Si DEPT and INEPT+ spectra and two-dimensional ^{1}H-^{29}Si and ^{1}H-^{1}H correlated spectroscopy (HSQC, HMBC, COSY). On the basis of these experiments, molecular connectivity consistent with four-bond ^{1}H-^{1}H coupling is confirmed.

Introduction

Proton-proton coupling is an essential diagnostic tool in the assignment of complex organic structures, particularly in the absence of X-ray crystallographic data. However, examples of structural insight arising from proton-proton coupling are rare for organosilanes. The comparative lack of examples of proton-proton coupling in organosilanes may reflect the greater stability of alkylsilanes over perhydrosilanes,[1,2] which increases distances between protons.[3] The most commonly documented proton-proton coupling relationships in organic compounds occur over relatively short ranges, such as geminal (two-bond coupling, ^{2}J) and vicinal (three-bond coupling, ^{3}J) coupling. An example of structural insight arising from proton-proton coupling is the Karplus equation,[4] which describes the correlation between vicinal proton-proton coupling ($^3J_{H\text{-}H}$) and dihedral torsion angles in organic compounds. Long-range proton-proton coupling is more unusual,[5–7] but W-coupling is an example of four-bond ($^4J_{H\text{-}H}$) coupling that is especially pronounced in carbocycles that constrain the coupled protons in a W-conformation (Figure 1a).[8,9]

We recently reported stereoselective syntheses of *cis*- and *trans*-siladecalins functionalized with Si-H bonds.[10] Carbocylic *cis*- and *trans*-decalin are classic examples in conformational analysis where the *cis* isomer is conformationally dynamic (capable of ring inversion), while the *trans* isomer is conformationally locked,[11,12] and these same configuration- and conformation-dependent distinctions were observed in the siladecalin scaffold. Among the spectroscopic consequences arising from these conformational differences is the observation of unusual splitting patterns in the 1-D ^{1}H NMR spectrum of *trans*-siladecalin (*trans*-$\mathbf{Si_{10}H_4}$, Figure 1b) that were not observed in *cis*-siladecalin (*cis*-$\mathbf{Si_{10}H_4}$) and were attributed to long-range W-coupling.

Herein, we describe the synthesis of cyclohexasilane **1** (Figure 1b) and identification of conditions yielding either diastereomer as the major product**.** Control of relative stereochemistry in the synthesis of silanes bearing multiple stereogenic centers is a significant challenge.[10,13] Our group has pioneered the use of H-labeled cyclosilanes as precursors to functionalized polysilanes.[14–18] Cyclosilane **1** was designed to probe long-range proton-proton coupling in organosilanes, as both stereoisomers can access the same W-conformation embedded within *trans*-$\mathbf{Si_{10}H_4}$ (Figure 1c). Interestingly, *cis*-**1** should have one additional W-coupled pathway relative to *trans*-**1**. We report detailed 1-D and 2-D NMR spectroscopic characterization of **1** supporting long-range proton-proton coupling in **1**.

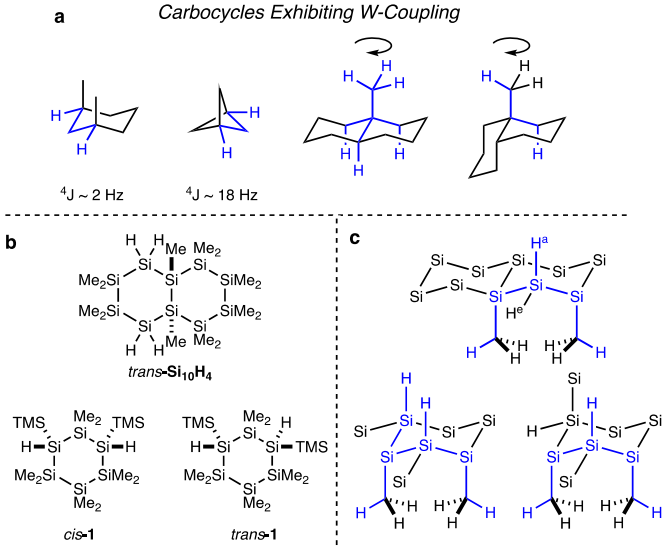

Figure 1. a) Examples of carbocyclic compounds with W-coupling pathways highlighted in blue. b) Cyclosilanes in this study. c) Select W-coupling pathways highlighted in blue for *trans*-$\mathbf{Si_{10}H_4}$ and *cis*- and *trans*-**1**.

[a] *Deprtment of Chemistry, Johns Hopkins University, 3400 N. Charles St, Baltimore, MD 21218*
† Current address: SciGenesis, 1100 Wicomico St, Suite 535, Baltimore, MD, 21230.
Electronic Supplementary Information (ESI) available: supplemental figures, NMR spectra, x-ray crystallography. See DOI: 10.1039/x0xx00000x

ARTICLE

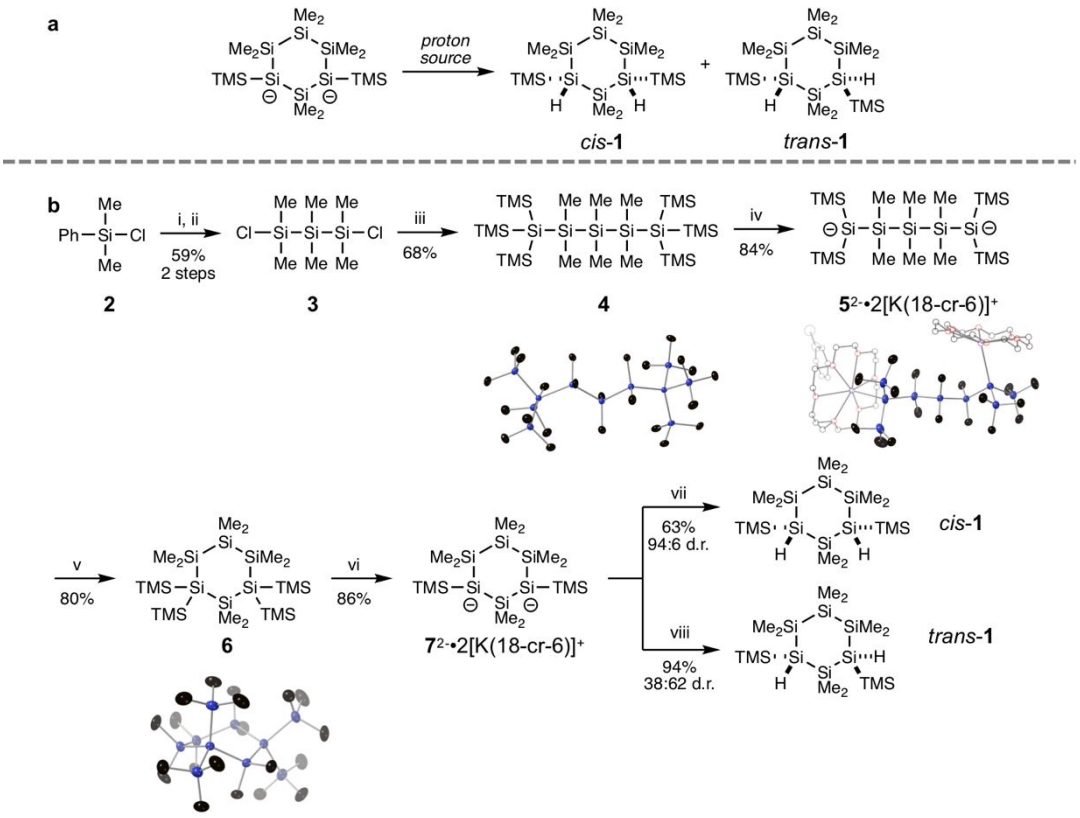

Scheme 1. a) Approach to the preparation of cyclosilane **1**. b) Synthesis from commercially available starting materials. X-ray crystal structures of key intermediates are shown. (i) Li, THF, 0 °C → rt, 24 h; *i*-PrMgCl, 0 °C, 30 min; $SiMe_2Cl_2$, 0 °C → rt, 15 h, 73%. (ii) $AlCl_3$, CH_3COCl, pentane, rt, 24 h, 81%. (iii) TMS_4Si, KO*t*-Bu, THF, rt, 2 h; then add **3**, 24 h, 68%. (iv) KO*t*-Bu, 18-cr-6, toluene, rt, 4 h, 84%. (v) $SiMe_2Cl_2$, toluene, rt, 24 h, 80%. (vi) KO*t*-Bu, 18-cr-6, toluene, rt, 4 h, 86%. (vii) $MgBr_2{\cdot}OEt_2$, toluene, rt, 15 min; MeOH, pentane, 15 min, 63%, 94:6 *cis*:*trans*. (viii) $MgBr_2{\cdot}OEt_2$, toluene, rt, 72 hr; 2M HCl in Et_2O, rt, 15 min, 94%, 38:62 *cis*:*trans*. Displacement ellipsoid plots (50% probability level at 110(2) K for compounds (5^{2-}•2[K(18-cr-6)]$^+$) and (7^{2-}•2[K(18-cr-6)]$^+$), at 130(2) K for compound **5**, and at 200(2) K for compound **6**). Black = carbon, blue = silicon, red = oxygen, purple = potassium. Hydrogens and disorder in countercations/solvent are omitted for clarity. Countercations and residual solvent are shown in wireframe.

Results and Discussion

Synthesis of Dianion 7^{2-}•2[K(18-cr-6)]$^+$.

We imagined preparing **1** via protonation of a 1,3-dianionic cyclosilane (Scheme 1a). Marschner synthesized a structurally isomeric 1,4-dihydrocyclosilane via dianion protonation.[19] The stereoselectivity of dianion protonation depends on dianion relative configuration as silyl anion protonation is stereoretentive.[20] Silyl anions are typically pyramidal,[21,22] although the configurational stability of silyl-substituted silyl anions is computationally predicted to be low.[23] Our synthetic plan therefore included characterization of the intermediate dianion's relative stereochemistry.

While the key 1,3-dianionic cyclosilane 7^{2-}•2[K(18-cr-6)]$^+$ was fortuitously previously reported,[24] as a synthetic intermediate, it was advanced without a reported yield and without discussion of relative stereochemistry. Additionally, some preceding synthetic steps were performed on milligram scale. We therefore developed a preparative scale synthesis of 7^{2-}•2[K(18-cr-6)]$^+$ (Scheme 1b). The synthesis proceeded in seven steps from commercially available starting materials. Due to some minor differences from reported NMR spectra, crystal structures were determined for several intermediates and are shown below the molecular structures.

Commercially available chlorodimethylphenylsilane ($ClSiMe_2Ph$, **2**) and dichlorodimethylsilane (Cl_2SiMe_2) were elaborated to known trisilane **3** by standard methods.[25,26] Potassio tris(trimethylsilyl)silane was formed *in situ* from tetrakis(trimethylsilyl)silane[27] and potassium *tert*-butoxide (KO*t*-Bu), then coupled to trisilane **3** to yield **4** in 68% yield.[28,29] bis-Desilylation of **4** with two equivalents of KO*t*-Bu/18-cr-6[28] formed acyclic dianion 5^{2-}•2[K(18-cr-6)]$^+$ in 84% yield. Addition of dichlorodimethylsilane[30] yielded the desired cyclosilane **6** in

80% yield. In the solid state, the central ring in **6** adopts a twist conformation, as previously reported.[30]

A second bis-desilylation with two equivalents of KO*t*-Bu/18-cr-6[24] converted **6** into dianion $\mathbf{7}^{2-}\bullet 2[K(18\text{-cr-}6)]^+$. This reaction proved significantly more complex than anticipated, as the trimethylsilyl tert-butoxide (TMSO*t*-Bu) formed during the reaction contributed to the formation of undesired by-products. It was found that the removal of the volatile TMSO*t*-Bu by application of dynamic vacuum[31] during dianion formation afforded greater selectivity for the desired product.

Single Crystal X-Ray Crystallography.

With the modified reaction conditions, $\mathbf{7}^{2-}\bullet 2[K(18\text{-cr-}6)]^+$ could be crystallographically characterized (Figure 2). Selected bond distances and angles are summarized in Table 1. Si–Si bond lengths were between 2.3–2.4 Å, which is typical for unstrained silanes (see Table S1 for complete data set). Only the *cis* diastereomer was observed and the trimethylsilyl groups adopted the equatorial positions. A single $[K(18\text{-cr-}6)]^+$ complex coordinated both anionic sites on one face of the molecule, while a second $[K(18\text{-cr-}6)]^+$ complex coordinated an ethereal oxygen atom. The combination of both contact and separated ion-pairing likely reflects the steric challenge of accommodating two $[K(18\text{-cr-}6)]^+$ complexes on one molecular face. Crown ether complexes of potassiosilanides are known to form separated ion pairs in the solid state.[32] The structurally isomeric 1,4-dianion $\mathbf{8}^{2-}\bullet 2[K(18\text{-cr-}6)]^+$ also adopted a chair conformation in the solid state with diequatorial TMS groups, but this led to a *trans*-diastereomer in which [K(18-cr-6)]+ complexes could engage in contact ion-pairing while on opposite faces of the cyclosilane plane (Scheme 2).[19]

The *cis* dianion is the precursor to *cis*-**1**. While only the *cis* isomer was observed in the solid state, chelation may be weaker in solution due to solvent stabilization of charged species. This could facilitate silyl anion stereochemical inversion, leading to *trans*-**1**.

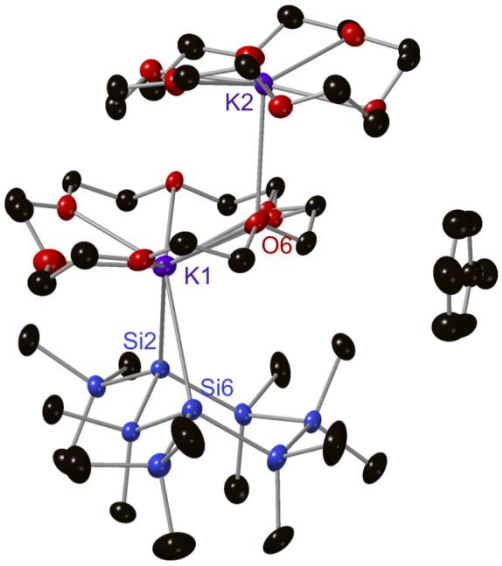

Figure 2. Displacement ellipsoid plots of dianion $\mathbf{7}^{2-}\bullet\mathbf{2}[K(18\text{-cr-}6)]$ (50% probability level) at 110(2) K. Black = carbon, blue = silicon, red = oxygen, purple = potassium. Hydrogens and disorder in crown ethers and lattice solvent molecules are omitted for clarity.

Table 1. Selected bond lengths (Å) and angles (deg) for dianion $\mathbf{7}^{2-}\bullet 2[K(18\text{-cr-}6)]$.

Bond lengths (Å)	
Si2-K1	3.5142(7)
Si6-K1	3.4989(8)
O6-K2	3.224(14)
Si-Si (avg)	2.339
Bond angles (deg)	
Si2-K1-Si6	64.274(16)

Dianion Protonation.

The results of a screen of protonation conditions are summarized in Table 2. Protonation of $\mathbf{7}^{2-}\bullet 2[K(18\text{-cr-}6)]^+$ with MeOH (Table 2, entry 1) resulted in decomposition to an insoluble product that was not characterized further. A reaction with a $MgBr_2\bullet OEt_2$ additive was more successful and provided **1** in 55% yield, with *cis*-**1** as the major product (74:26 *cis:trans*, entry 2). Exchanging MeOH for HCl as the proton source had a minimal effect on d.r. but increased isolated yield to 96% (entry 3). The observation of significant quantities of *trans*-**1** despite observation of a single diastereomer in the solid state points to a mechanism for silyl anion stereochemical inversion in solution.

Ultimately, the reaction time between $\mathbf{7}^{2-}\bullet 2[K(18\text{-cr-}6)]^+$ and $MgBr_2\bullet OEt_2$ (entries 3-5) emerged as a significant influence on d.r., with more *trans*-**1** observed with longer reaction times. The highest d.r. favoring *trans*-**1** (38:62 *cis:trans*) was observed with a 72 h reaction time (entry 5).

Table 2. Dianion protonation diastereoselectivity.

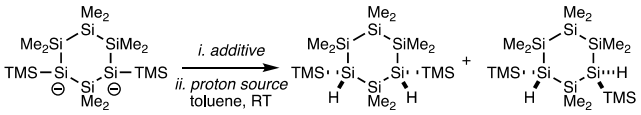

Entry	Additive	Proton Source	Yield (%)	dr (*cis*:*trans*)
1	–	MeOH	–	–
2	$MgBr_2\bullet OEt_2$, toluene, 30 min	MeOH, 30 min	55	74:26
3	$MgBr_2\bullet OEt_2$, toluene, 30 min	HCl, 30 min	96	73:27
4	$MgBr_2\bullet OEt_2$, toluene, 24 h	HCl, 30 min	97	49:51
5	$MgBr_2\bullet OEt_2$, toluene, 72 h	HCl, 30 min	94	38:62
6	$MgBr_2\bullet OEt_2$, pentane, 16 h	MeOH/ pentane, 15 min	63	94:6

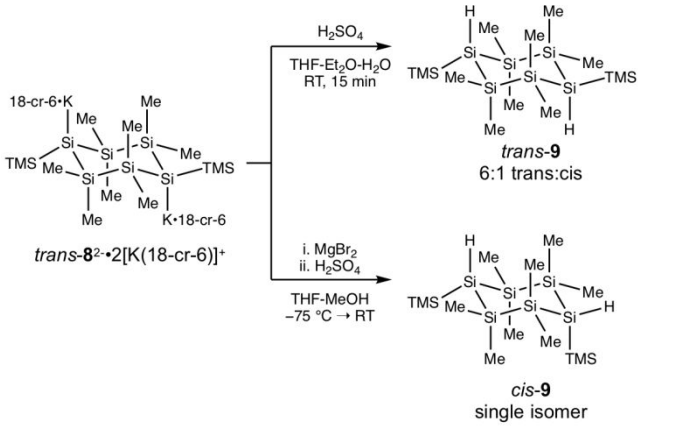

Scheme 2. Prior work by Marschner on stereoselective dianion protonation via countercation effects.[19]

These initial observations pointed to a different mechanism for stereocontrol than advanced in a prior study of 1,4-dianion **8**$^{2-}$•2[K(18-cr-6)]$^{+}$ protonation.[19] Marschner et al. identified a strong influence of the countercation on d.r., with *trans*-**8**$^{2-}$•2[K(18-cr-6)]$^{+}$ yielding predominantly cyclosilane *trans*-**9** (6:1 *trans:cis*, Scheme 2), while a magnesium congener yielded only *cis*-**9**. This was attributed to different rates of silyl anion stereochemical inversion in an intermediate monoanion depending on the countercation: rapid epimerization of an intermediate potassium monoanion and slow epimerization of the magnesium monoanion.

In contrast, we find that the magnesium dianion can yield either the *cis* or the *trans* product. Critically, we also find that stereochemical control *occurs prior to addition of a proton source*, which implies equilibration of *cis* and *trans* dianions. Only the bridged contact ion pair *cis*-**7**$^{2-}$•2[K(18-cr-6)]$^{+}$ was observed in the solid state (Figure 2), supporting the plausibility of a species similar to *cis*-**7**$^{2-}$•Mg^{2+} (Scheme 3) as the precursor to *cis*-**1**. Due to the cyclic structure, *cis*-**7**$^{2-}$•Mg^{2+} cannot undergo epimerization without breaking the Si–Mg contact. We suggest that the increase in *trans*-**1** over long reaction times between dianion and $MgBr_2$ is consistent with enrichment in the concentration of a species similar to *trans*-**7**$^{2-}$•Mg^{2+}, where the Mg^{2+} cation no longer bridges both anionic Si sites. A solvent-separated or higher-order assembly (e.g. coordination polymer) might be implicated in the structure of *trans*-**7**$^{2-}$•Mg^{2+}. The equilibration of intermediate monoanions (e.g. *cis*- and *trans*-**10**$^{-}$•MgX) may also influence the ultimate product distribution.

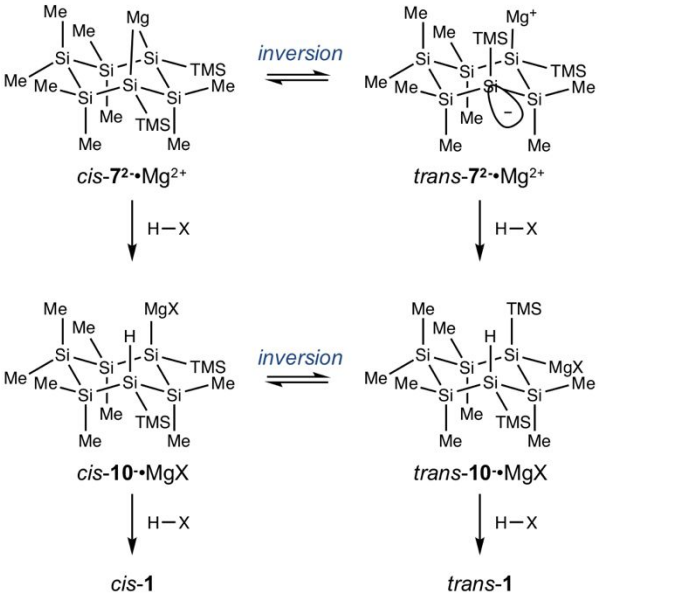

Scheme 3. Hypothesized pathways for dianion protonation.

Given the possibility that solvent influences the relative concentration of diastereomeric dianions, we revisited protonation conditions. Exchanging toluene for pentane in combination with methanol as proton source (entry 6) increased the *cis:trans* selectivity to 94:6, the highest diastereoselectivity in favor of either isomer observed in this study. Isomerically pure samples of each diastereomer were not isolated. **1** was an oil at room temperature, prohibiting stereochemical enrichment by recrystallization as well as isolation of X-ray quality crystals. The stereoisomers were not chromatographically separable on silica gel. The lack of an x-ray structure also complicated assignment of the diastereomers, a challenge ultimately resolved by NMR spectroscopy (vide infra).

1-D ^{1}H and ^{29}Si NMR spectroscopy of 1.

Examples of one-dimensional ^{1}H and ^{29}Si NMR spectra of **1** are shown in Figures 3-4. Each figure is labeled with the structure of both diastereomers as well as peak assignments. The final assignments, chemical shifts and experimentally observed multiplets and coupling constants are summarized in Table 3. The logic for peak assignments follows below. The atom numbering scheme was adopted by analogy to Tamao.[33]

The 1-D ^{29}Si {^{1}H} DEPT (distortionless enhancement by polarization transfer) spectrum of **1** showed five resonances for each isomer (Figure 3). Si-1 and Si-5 were assigned on the basis of the distinct chemical shifts of hydrogenated and trimethylated silanes, while the three -$SiMe_2$- resonances clustered between δ -30 and -45. The proton-coupled ^{29}Si INEPT+ spectrum (Figure S1) confirmed the Si-1 assignments in *cis*-**1** to δ -109.3 and Si-1, Si-1' in *trans*-**1** to δ -109.5 due to observation of the large one-bond proton-silicon coupling ($^{1}J_{Si-H}$ 160 Hz). The resonance assigned to Si-5 also showed the expected multiplet arising from two-bond coupling (e.g. $^{2}J_{Si-C-H}$) to three attached methyl groups. The remaining assignments for Si-2, Si-3, and Si-4 were made on the basis of the

multiplicities expected for two- and three-bond proton-silicon coupling (Figure S2 and Table S2).[34]

Table 3. ^{1}H and ^{29}Si NMR chemical shifts (ppm), apparent multiplets, and J (Hz) for *cis*- and *trans*-1.

cis-***1***		*trans*-***1***	
^{29}Si NMR		*^{29}Si NMR*	
Si-1	-109.3	Si-1, Si-1’	-109.5
Si-2	-37.3	Si-2, Si-2’	-38.7
Si-3	-40.6	Si-3	-41.6
Si-4	-33.4	Si-4	-35.1
Si-5	-8.35	Si-5, Si-5’	-8.95
^{1}H NMR		*^{1}H NMR*	
H-1	2.807 (s)	H-1, H-1’	2.777 (s)
Me-5	0.295 (s)	Me-5, Me-5’	0.302 (s)
Me-2β	0.408 (s)	Me-2β, Me2’α	0.383 (s)
Me-2α	0.336 (d, 0.66)	Me-2α, Me-2’β	0.388 (d, 0.55)
Me-3β	0.239 (s)	Me-3α, Me-3β	0.258 (s)
Me-3α	0.349 (s)	Me-4α, Me-4β	0.515 (d, 0.44)
Me-4β	0.565 (s)		
Me-4α	0.422 (t, 0.7)		

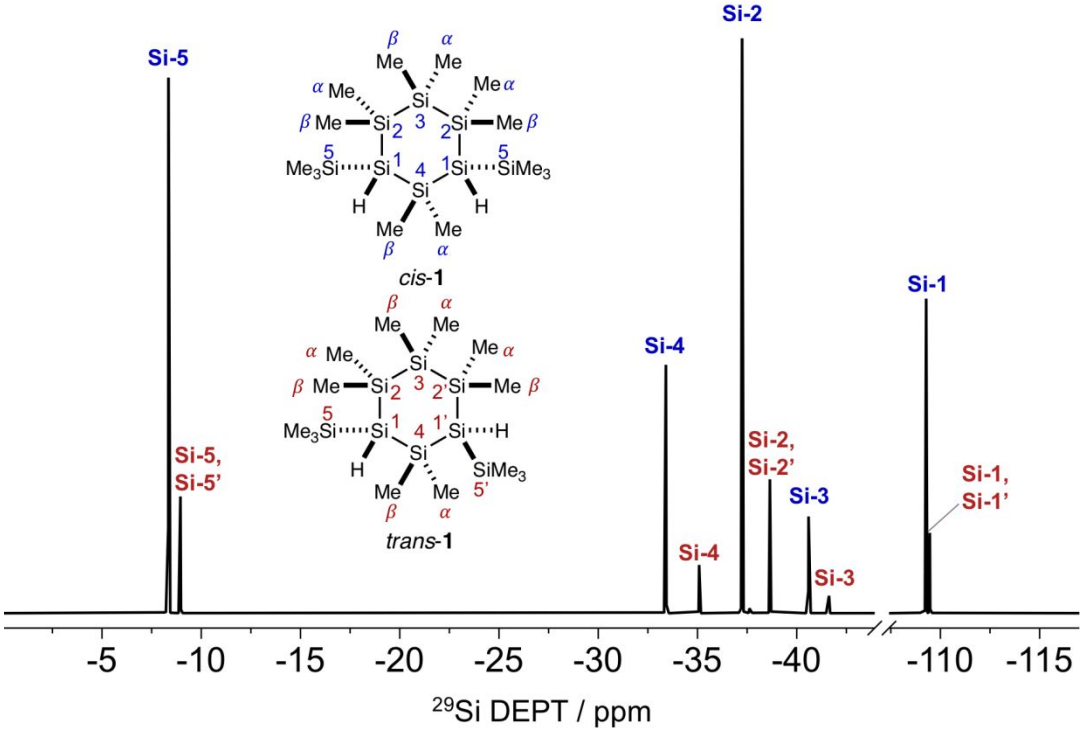

Figure 3. ^{29}Si {^{1}H} DEPT NMR spectrum (79 MHz, C_6D_6) of **1** (83:17 *cis:trans*). Assignments are indicated. Peaks corresponding to the major isomer *cis*-**1** are labeled in blue and peak corresponding to the minor isomer *trans*-**1** are labeled in red.

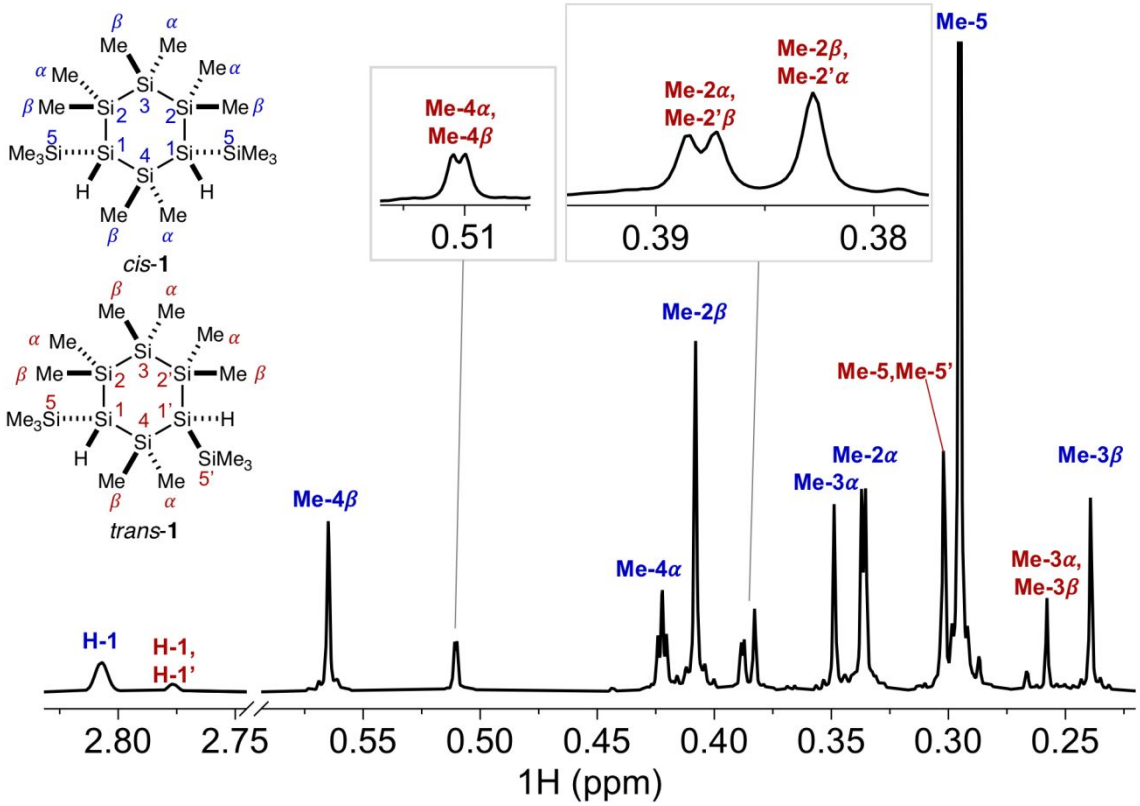

Figure 4. Cropped ^{1}H NMR spectrum (400 MHz, C_6D_6) of **1** (83:17 *cis:trans*). Assignments are indicated. Peaks corresponding to the major isomer *cis*-**1** are labeled in blue and peak corresponding to the minor isomer *trans*-**1** are labeled in red.

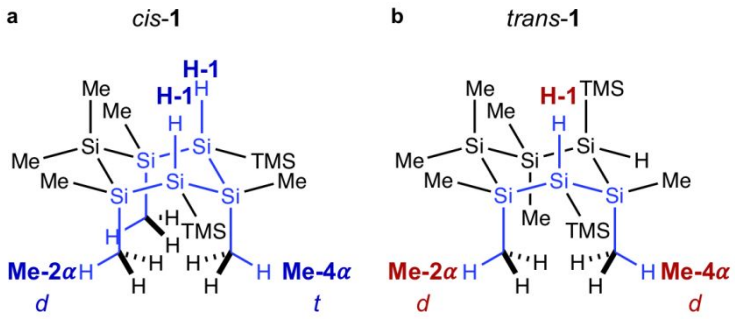

Figure 5. Proposed W-coupled protons in chair conformations of a) *cis*- and b) *trans*-**1**.

The diastereomeric ratio was determined by integration of the ^{1}H NMR spectrum (Figure 4). The major and minor isomers could be assigned to *cis*- and *trans*-**1** respectively on the basis of each isomer's distinct symmetry (Figure S3) and the consequences on the expected number of peaks in their ^{1}H NMR spectra. As is typical for cyclic molecules, symmetry elements were determined from the highest symmetry planar conformation even when multiple low-energy conformers may exist.[35] We determined that *cis*-**1** is C_s-symmetric (*meso*). The mirror plane of symmetry that relates both halves of the molecule resulted in eight expected ^{1}H NMR resonances. In contrast, *trans*-**1** was determined to be C_2-symmetric, which renders substituents on atoms along the central axis of symmetry to be chemically equivalent, resulting in six expected resonances. Substituents are labeled according to the silicon atom number. Methyl groups on the cyclosilane were labeled as α if below the plane of the cyclosilane and β if above the plane.

A notable feature of the ^{1}H NMR spectrum (Figure 4) was that several resonances at chemical shifts typical of methylsilane groups appeared as doublets or triplets, despite the absence of geminal or vicinal hydrogen atoms. In addition, the silane hydrogen (H-1) apparent singlet was significantly broadened.

These observations appeared consistent with the W-coupling *cis*- and *trans*-**1** were designed to probe. Considering the chair conformation of *cis*-**1** in which the bulky TMS groups adopt the equatorial position (Figure 5a), the diaxial silane hydrogens (H-1) are in an appropriate conformation to couple to two different protons in the neighboring axial methyl groups (Me-2α and Me-4α). Me-4α would couple to the two chemically equivalent diaxial SiH's (H-1), while Me-2α would couple only to H-1. By this first-order analysis, Me-2α is an expected doublet and Me-4α an expected triplet.

This first-order analysis neglects potential second-order effects arising from magnetic inequivalence.

In the experimental 1-D ^{1}H NMR spectrum of *cis*-**1**, the δ 0.422 triplet and δ 0.336 doublet have the predicted coupling patterns and an experimentally observed coupling constant (J ~ 0.7 Hz) on the order of W-coupling observed in constrained cyclohexanes ($^4J_{H\text{-}H}$ = 0-2 Hz).[36] These resonances were therefore preliminarily assigned to Me-4α and Me-2α respectively. All other resonances were apparent singlets.

Considering the chair conformation of *trans*-**1** (Figure 5b), the same W-pathways between an axial silane hydrogen (H-1) and neighboring axial methyl groups (Me-2α and Me-4α) were identified, although Me-4α is predicted to appear as a doublet because only one Si-H is axial. The δ 0.515 and δ 0.388 resonances were apparent doublets and were preliminarily assigned to Me-4α and Me-2α respectively. In the minor isomer, all other resonances were apparent singlets. The extensive coupling to multiple protons could account for the unusually broad Si*H* resonances in both isomers.

To establish these preliminary assignments and hypothesized W-coupling on firmer ground, we pursued two-dimensional spectra that could more definitively establish connectivity and coupling.

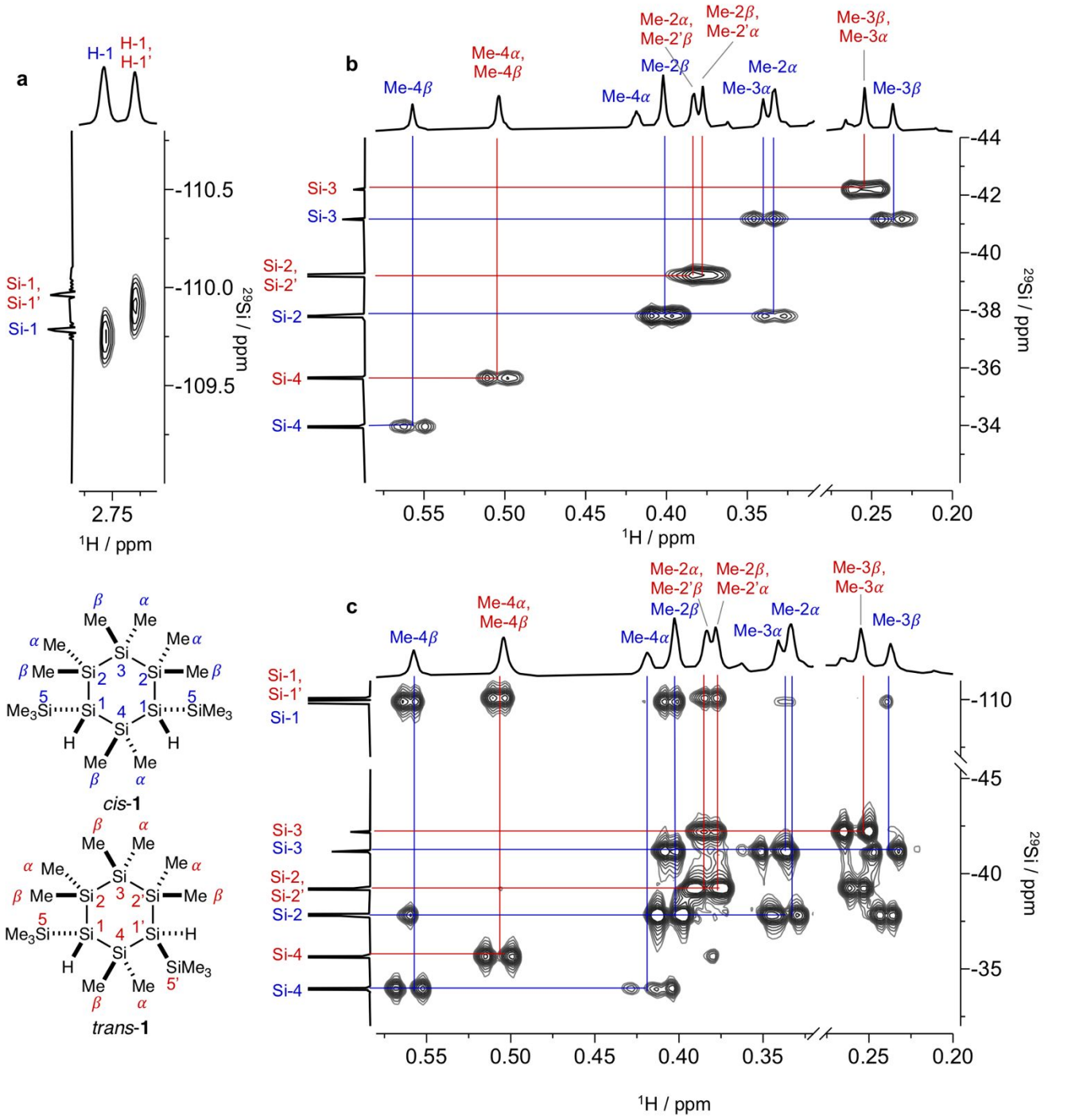

Figure 6. a) Cropped ^{1}H-^{29}Si HSQC showing single bond correlations (*cis*-**1**: H-1 connected to Si-1; *trans*-**1**: H-1,H-1' connected to Si-1,Si-1'). b) Cropped ^{1}H-^{29}Si HMBC ($J_{H\text{-}Si}$ = 3 Hz) showing most two-bond correlations consistent with Me groups attached to Si-2, Si-3, and Si-4. c) Cropped ^{1}H-^{29}Si HMBC ($J_{H\text{-}Si}$ = 7 Hz) showing two-, three- and some four-bond correlations consistent with Me groups attached to Si-2, Si-3, and Si-4.

2-D NMR spectroscopy of 1.

2-D ^{1}H-^{29}Si HSQC and HMBC spectra allowed assignment of all methyl groups to specific attached silicon atoms. ^{1}H-^{29}Si heteronuclear single quantum coherence (HSQC) detects one-bond correlations and confirmed that protons at δ 2.81 and δ 2.78 are directly attached to Si-1 (*cis*-**1**) and Si-1, Si-1' (*trans*-**1**) (Figure 6a).

^{1}H-^{29}Si heteronuclear multiple bond correlation (HMBC) spectroscopy detects longer range correlations, such as correlations across two- or three-bonds. As long-range coupling constants between ^{1}H and ^{29}Si are not all the same and vary with distance, several spectra with different values of $J_{H\text{-}Si}$ were collected (3 Hz, 7 Hz, and 10 Hz). A correlation table (Table 4) summarizes the number of bonds between expected ^{1}H-^{29}Si

correlations for Me-2, Me-3, and Me-4 resonances. Correlations across distances longer than four-bonds were omitted.

The 3 Hz spectrum (Figure 6b) showed almost all two-bond correlations. No longer range correlations were observed. This allowed direct assignment of all methyl resonances but one. While a cross-peak for one *cis*-**1** resonance (δ 0.42) was not observed, by process of elimination this was assigned to Me-4.

The 7 Hz spectrum (Figure 6c) showed all two- and three-bond correlations, as well as some four-bond resonances. The cross-peaks between *cis*-**1**'s Me-4 resonances are discussed first. Cross-peaks were observed between the δ 0.57 and δ 0.42 resonances in the ^{1}H NMR spectrum and Si-4, consistent with the assignment to Me-4β or Me-4α. Two cross-peaks were also observed with Si-1, consistent with three-bond Me-4β/Si-3 or Me-4α/Si-3 correlations. Two cross-peaks attributed to four-bond correlations were also identified: a Me-4α/Si-2 and a Me-2β/Si-4 correlation, the latter of which partially overlapped the two-bond Me-4α/Si-4 correlation.

Table 4. Expected correlations for select methyl resonances in *cis*- and *trans*-**1** showing the number of bonds for each correlation. Correlations longer than four-bond are omitted.

Cis-**1**			
Si/H	*Me-2*	*Me-3*	*Me-4*
Si-1	3	4	3
Si-2	2	3	4
Si-3	3	2	–
Si-4	4	–	2
Si-5	4	–	4

Trans-**1**				
Si/H	*Me-2*	*Me-2'*	*Me-3*	*Me-4*
Si-1	3	–	4	3
Si-1'	–	3	4	3
Si-2	2	4	3	4
Si-2'	4	2	3	4
Si-3	3	3	2	–
Si-4	4	4	–	2
Si-5	4	–	–	4
Si-5'	–	4	–	4

Similar analyses supported the assignment of the remaining methyl resonances in *cis*- and *trans*-**1**. Methyl groups attached to Si-3 showed strong correlations to Si-3 (two-bond) and Si-2 (three-bond), but weak or no correlations to Si-1 (four-bond). Methyl groups attached to Si-2 are distinguished by having three strong cross-peaks consistent with one two-bond correlation (e.g. *cis*-**1**: Me-2β/Si-2) and two three-bond correlations (e.g. *cis*-**1**: Me-2β/Si-3 and Me-2β/Si-1). Copies of full spectra and a 10 Hz HMBC spectrum are included in the Supporting Information (Figures S4-S7).

The heteronuclear correlated spectra showed the correct connectivity for long-range proton-proton coupling to account for the multiplets assigned to Me-2α and Me-4α, but HSQC and HMBC do not directly distinguish diastereotopic methyl groups: for example, the HMBC spectra showed that the δ 0.57 singlet and δ 0.42 triplet were both attached to Si-4 in *cis*-**1**, but cannot distinguish which is Me-4α (below plane) or Me-4β (above plane). Unfortunately, NMR methods (e.g. NOESY) used for determination of relative stereochemistry in organic compounds were of limited utility for cyclosilane **1.** NOESY (Nuclear Overhauser Effect Spectroscopy) data can distinguish between geminal and vicinal protons in cyclohexane derivatives on the basis of large differences in NOE integrals arising from significant differences in interproton distances.[37] However, the differences between cyclohexanes and cyclohexasilanes with respect to bond lengths and dynamic properties limit the utility of NOESY for methylated cyclosilanes.[38] For example, in the crystal structure of $\mathbf{7}^{2-}\bullet 2[K(18\text{-cr-}6)]^+$, the interproton distance between methyl groups on the same silicon atom differed from interproton distances between adjacent silicon atoms by only 0.1 Å (Figure S8). The average through-space distances between protons on geminal and vicinal methyl groups in a methylated cyclohexasilane are likely much more similar than observed for geminal and vicinal protons on a cyclohexane.

Distinguishing α and β methyl groups on the same Si atom in **1** therefore depends on proton-proton coupling. If W-coupling accounts for the splitting patterns observed in the ^{1}H NMR spectrum, cross-peaks between H-1 and the methyl resonances indicated in Figure 5 should be observed by correlated spectroscopy (COSY). We therefore obtained a ^{1}H-^{1}H gCOSY (gradient-selected COSY) spectrum of **1**.

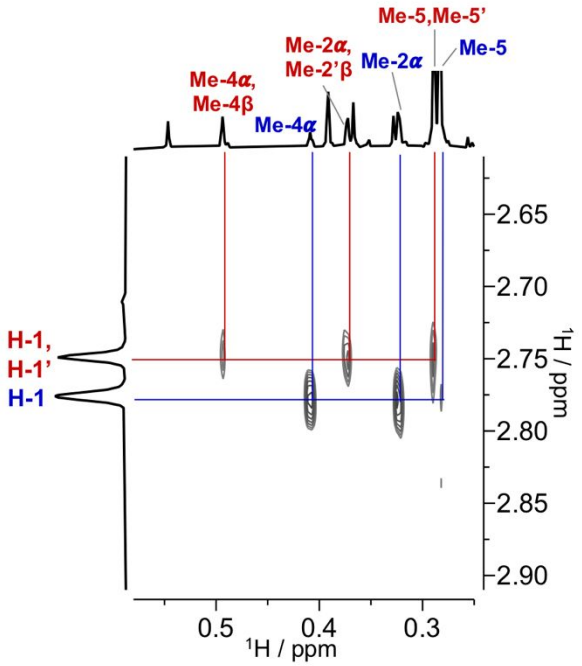

Figure 7. Cropped ^{1}H-^{1}H gCOSY (400 MHz, C_6D_6) spectrum of **1** (55:45 *cis:trans*). Peaks assigned to *cis*-**1** are labeled in blue and peaks assigned to *trans*-**1** are labeled in red.

The combination of heteronuclear correlated spectroscopy and gCOSY unambiguously confirm that long-range, four-bond proton-proton coupling accounts for the multiplets observed in both diastereomers. Cross-peaks were observed between the Si–H resonances and methyl groups attached to Si-2 and Si-4 in both *cis*- and *trans*-**1** (Figure 7). A full spectrum is included in the supporting information (Figure S9).

With respect to Me-2 and Me-4 resonances, only one methyl group of two attached to the same Si atom coupled to H-1. This *configuration*-dependent four-bond coupling can be explained by *conformation*-dependent W-coupling (Figure 5) where only one methyl group has the optimal alignment for four-bond coupling. On the basis of these data, the diastereotopic Me-4α/Me-4β and Me-2α/Me-2β signals in *cis*- and *trans*-**1** were assigned. Cross-peaks were also observed between H-1 and the trimethylsilyl groups (*cis*-**1**: H-1/Me-5; *trans*-1: H-1/Me-5,Me-5'), long-range coupling that was not apparent from inspection of the 1-D ^{1}H NMR spectrum. W-conformations exist for the H-1/Me-5 pair as well.

These data constitute an unusual example of long-range proton-proton coupling playing a role in structural elucidation of a complex oligosilane. As a counterpoint illustrating the utility of long-range coupling, we discuss the example of the Me-3 signals in *cis*-**1**. While in C_2-symmetric *trans*-**1** the substituents on atoms along the rotational axis are chemically equivalent by symmetry, in C_s-symmetric *cis*-**1** the methyl groups attached to Si-3 (falling along the mirror plane) are chemically inequivalent. The protons of Me-3α and Me-3β appear as singlets in the ^{1}H NMR spectrum, are at least five bonds distant from any other proton, and therefore these diastereotopic groups cannot be distinguished on the basis of configuration- and conformation-dependent proton-proton coupling. The assignments shown in Table 3 and Figure 4 were instead based on the observation that axial methyl substituents in cyclohexane[39–41] and cyclosilane[42] rings fall at lower frequency chemical shifts than equatorial methyl groups, a trend reproduced by the Me-2α/Me-2β and Me-4α/Me-4β pairs as well.

Conclusions

Cyclosilane **1** is a mixed methyl- and hydro-labeled oligosilane that possesses *cis/trans* stereoisomerism. We synthesized **1** in a seven-step sequence culminating in a key dianion protonation that determined relative stereochemistry. Protonation conditions yielding either diastereomer as the major product were identified. X-ray crystal structures of key intermediates, including the cyclic dianion $\mathbf{7}^{2-}\bullet 2[K(18\text{-cr-}6)]^+$, were unambiguously determined. Our results support the utility of dianions as precursors to complex, functional silanes.[43–46]

Each isomer is a probe of long-range proton-proton coupling, as conformational differences result in differential access to the W-conformation that maximizes four-bond (^{4}J) long-range coupling. We analyzed both 1-D and 2-D NMR spectra to assign connectivity and more firmly establish long-range coupling. Additionally, we show that 2-D NMR spectroscopy is a tool for identification of long range ^{1}H-^{1}H coupling that may be difficult to observe by 1D ^{1}H NMR due to a small coupling constants that result in significant line broadening. These results point to the utility of NMR spectroscopy for structure determination in complex, stereochemically rich main group heterocycles, especially for liquid or amorphous materials not suitable for X-ray crystallography.

As the field of main group synthesis advances, target structural complexity grows. With increasingly complex materials, the need for sophisticated structural characterization also grows. The case study herein demonstrates characterization of both molecular connectivity and relative stereochemistry in a small but complex cyclic silane. This study may guide future structural characterization of complex main group molecular and polymeric materials.

Experimental

General information

Reactions were performed either using standard Schlenk line techniques under a dry argon atmosphere or in a UNIlab Plus Glove Box by MBRAUN under a dry nitrogen atmosphere. All glassware was oven-dried overnight at 175 °C. All reaction solvents were dried and degassed on a J. C. Meyer Solvent Dispensing System. All chemicals were obtained from commercial suppliers and used without further purification. The following compounds were previously reported: **3**,[25] **4**,[28] $\mathbf{5}^{2-}\bullet 2[K(18\text{-cr-}6)]^+$,[28] **6**,[30] and $\mathbf{7}^{2-}\bullet 2[K(18\text{-cr-}6)]^+$.[24] Compound **3** was prepared according to literature procedure without further modification. Modified syntheses of **4**, $\mathbf{5}^{2-}\bullet 2[K(18\text{-cr-}6)]^+$, **6**, and $\mathbf{7}^{2-}\bullet 2[K(18\text{-cr-}6)]^+$ are described below. For compounds **4**, $\mathbf{5}^{2-}\bullet 2[K(18\text{-cr-}6)]^+$, **6**, and $\mathbf{7}^{2-}\bullet 2[K(18\text{-cr-}6)]^+$, spectroscopic and crystallographic data are provided to confirm identity due to minor differences from reported data.

Chemical Synthesis

2,2,6,6-tetrakis(trimethylsilyl)dodecamethylheptasilane (**4**). Inside a glovebox, a solution of TMS_4Si (2.90 g, 9.00 mmol, 2.00 equiv.) in THF (10.0 mL) was added dropwise to a solution of KO*t*-Bu (1.01 g, 2.00 equiv., 9.00 mmol) in THF (25.0 mL) in a 100 mL Schlenk flask and stirred for 3 hours at room temperature. The solution immediately turned orange. $MgBr_2{\cdot}OEt_2$ (2.33 g, 2.00 equiv., 9.00 mmol) was added as a solid and the solution was allowed to stir for 30 minutes as it became a translucent yellow color. A solution of dichlorohexamethyltrisilane (**3)** (1.11 g, 1.00 equiv., 4.52 mmol) in THF (5.0 mL) was added dropwise and a white precipitate was observed. The solution was removed from the glovebox and allowed to stir on the Schlenk line for 24 hours before aqueous sulfuric acid (0.5 M, 5 mL) was added dropwise by pipette. The biphasic mixture was transferred to a separatory funnel and additional aqueous sulfuric acid (0.5 M, 95 mL) was added. The aqueous and organic layers were separated. The aqueous layer was extracted three times with Et_2O (3 x 50 mL). The combined organic layers were dried over anhydrous Na_2SO_4, filtered, and concentrated on a rotary evaporator. The reaction mixture was dissolved in a minimum volume of boiling Et_2O and five times this quantity of room-temperature acetone was slowly added to precipitate crystals suitable for X-ray diffraction studies. Yield: 2.10 g, 3.14 mmol, 70%. δ ^{1}H NMR (400 MHz, C_6D_6) 0.52 (18H, m) 0.34 (54H, s). δ ^{13}C NMR (101 MHz, C_6D_6) 3.65, 1.11, -1.76. δ ^{29}Si NMR (79 MHz, C_6D_6) -9.32, -29.83, -36.88, -127.91.

1,5-dipotassio-1,5-bis(trimethylsilyl)hexamethylpentasilane ($\mathbf{5}^{2-}\bullet 2[K(18\text{-cr-}6)]^+$). A solution of KO*t*-Bu (0.786 g, 2.00 equiv., 7.00 mmol) and 18-crown-6 (1.85 g, 2.00 equiv., 7.00 mmol) in toluene (70 mL) was prepared inside a 250 mL Schlenk flask

inside a glovebox. A solution of oligosilane **4** (2.35 g, 1.00 equiv., 3.50 mmol) in toluene (70 mL) was added by syringe to the KO*t*-Bu/18-cr-6 solution and the reaction mixture stirred for 30 minutes at room temperature. The reaction mixture was warmed in a water bath to 30 °C and solvent was removed by vacuum pump (3.00 Torr) over the course of 3 hours. Additional toluene (60 mL) was added and the reaction mixture was heated to 70 °C until all material dissolved. The reaction mixture was removed from the water bath and pentane (150 mL) was layered on top of the solution by syringe. Yellow crystals precipitated out of the solution overnight and were collected by filtration before being washed with 50 mL pentane. Yield: 3.47 g, 3.07 mmol, 88%. δ ^{1}H NMR (400 MHz, C_6D_6) 3.23 (48 H, s), 0.99 (12 H, s), 0.79 (42 H, m). δ ^{13}C NMR (101 MHz, C_6D_6) 70.12, 8.66, 7.79, 5.56. δ ^{29}Si NMR (79 MHz, C_6D_6) -3.78, -22.43, -39.73, -184.14.

1,1,3,3-tetrakis(trimethylsilyl)-octamethylcyclohexasilane (**6**). A yellow solution of $\mathbf{5}^{2-}$•2[K(18-cr-6)]$^{+}$ (3.47 g, 1.00 equiv., 3.07 mmol) in toluene (120 mL) was prepared at 70 °C and allowed to cool to room temperature. A solution of $SiMe_2Cl_2$ (0.38 mL, 1.0 equiv., 3.1 mmol) in toluene (8.0 mL) was added dropwise by syringe to the yellow solution of $\mathbf{5}^{2-}$•2[K(18-cr-6)]$^{+}$ and stirred for 2 hours at room temperature. The solution slowly became colorless. Dilute aqueous H_2SO_4 (0.5 M, 5 mL) was added dropwise by pipette and the biphasic mixture was transferred to a separatory funnel. Additional aqueous H_2SO_4 (0.5 M, 95 mL) was poured into the funnel and the aqueous and organic layers were separated. The aqueous layer was extracted three times with Et_2O (3 x 100 mL). The combined organic layers were dried over anhydrous Na_2SO_4, filtered, and concentrated on a rotary evaporator. The crude product was dissolved in 15 mL of Et_2O heated to its boiling point and upon cooling crystals suitable for X-ray diffraction were obtained. Yield: 1.45 g, 2.49 mmol, 80%. δ ^{1}H NMR (400 MHz, C_6D_6) 0.58 (6H, s), 0.41 (12H, s), 0.36 (36H, s), 0.25 (6H, s). δ ^{13}C NMR (101 MHz, C_6D_6) 5.36, 4.48, -0.47, -5.51. δ ^{29}Si NMR (79 MHz, C_6D_6) -8.03, -30.01, -39.48, -45.08, -125.35.

1,3-dipotassium-1,3-bis(trimethylsilyl)-octamethylcyclohexasilane ($\mathbf{7}^{2-}$•2[K(18-cr-6)]$^{+}$). In a glovebox a solution of KO*t*-Bu (0.781 g, 2.00 equiv., 6.96 mmol) and 18-crown-6 (1.84 g, 2.00 equiv., 6.96 mmol) in toluene (70 mL) was prepared inside a 250 mL Schlenk flask. A solution of oligosilane **6** (2.02 g, 1.00 equiv., 3.47 mmol) in toluene (70 mL) was added by syringe to the KOt-Bu/18-cr-6 solution and the reaction mixture stirred for 30 minutes at room temperature. The reaction mixture was warmed in a water bath to 30 °C and solvent was removed by vacuum pump over the course of 3 hours. Additional toluene (60 mL) was added and the reaction mixture was heated to 70 °C until all material dissolved. The reaction mixture was removed from the water bath and pentane (150 mL) was layered on top of the solution by syringe. Yellow-orange crystals precipitated out of the solution overnight and were collected by filtration before being washed with 50 mL pentane. Yield: 3.13 g, 2.92 mmol, 86%. δ ^{1}H NMR (400 MHz, C_6D_6) 3.32 (48 H, s), 1.04 (6 H, s), 0.92 (12 H, s), 0.81 (18 H, s), 0.69 (6 H, s). δ ^{13}C NMR (101 MHz, C_6D_6) 69.74, 14.10, 9.16, 4.64, -4.50. δ ^{29}Si NMR (79 MHz, C_6D_6) -7.52, -29.50, -38.97, -44.57, -124.81.

1,3-bis(trimethylsilyl)-1,3-dihydrooctamethylcyclohexasilane (*cis*-**1**). Inside a glove box, a suspension of $MgBr_2$·OEt_2 (0.2 M, 0.163 g, 2.70 equiv., 0.631 mmol) in toluene (3.00 mL) was added by pipet to a solution of $\mathbf{7}^{2-}$•2[K(18-cr-6)]$^{+}$ (0.013 M, 0.253 g, 1.00 equiv., 0.226 mmol) in toluene (18.0 mL) which stirred for 15 minutes. A tan solid precipitated. Volatiles were removed under vacuum (5 Torr), after which pentane (21.0 mL) was added. The mixture stirred for 16 hours. Methanol (25.0 µL, 2.77 equiv., 0.618 mmol) was then added directly to the suspension to give a colorless solution with a white precipitate. 15 minutes later the solution was filtered through packed Celite with additional pentane (3 x 50 mL) used to wash the precipitate. Removing the solvent from the filtrate gave the crude product. Yield: 57.4 mg, 0.131 mmol, 63% (94:6 *cis*:*trans*) δ ^{1}H NMR (400 MHz, C_6D_6) 2.81 (2 H, br), 0.56 (3 H, s), 0.42 (3 H, t), 0.41 (6 H, s), 0.35 (3 H, s), 0.34 (6 H, d), 0.30 (18 H, s), 0.24 (3 H, s). δ ^{13}C NMR (101 MHz, C_6D_6) 2.76, 2.29, -0.57, -2.36, -2.91, -6.00, -7.32. δ ^{29}Si NMR (79 MHz, C_6D_6) -8.35, -33.41, -37.25, -40.60, -109.28. IR (ATR) ν_{max}/cm^{-1}: 2947 and 2891 (CH), 2052 (SiH), 1401, 1244 (Si-CH_3), 909, 835, 803, 780, 747, 730, 687, 646, 614, 466, 425. HRMS (EI) m/z: calculated for $C_{14}H_{42}Si_8$ [M-H_2] 434.1441, found 434.1440.

1,3-bis(trimethylsilyl)-1,3-dihydro-octamethylcyclohexasilane (*trans*-**1**). Inside a glovebox, $MgBr_2$·OEt_2 (0.220 g, 2.1 equiv., 0.85 mmol) was added directly to a solution of **7**•2[K(18-cr-6)]$^{+}$ (0.455 g, 1.00 equiv., 0.400 mmol) in toluene (40.0 mL). A tan solid precipitated. The mixture was stirred for 3 days at room temperature. HCl (2 M in Et_2O, 0.400 mL, 2 equiv., 0.800 mmol) was added directly to the suspension to give a colorless solution with a white precipitate. After 30 minutes, pentane (100 mL) was added to the flask and the solution became cloudy. The solution was filtered through packed Celite using additional pentane (3 x 50 mL) to wash the precipitate. The solvent was removed from the filtrate to obtain a crude product. Yield: 167 mg, 0.382 mmol, 94% (38:62 *cis*:*trans*) δ ^{1}H NMR (400 MHz, C_6D_6) 2.78 (2 H, br), 0.51 (6 H, d), 0.39 (6 H, d), 0.38 (6 H, s), 0.30 (18 H, s), 0.26 (6 H, s). δ ^{13}C NMR (101 MHz, C_6D_6) 2.55, 1.53, -2.04, -2.73, -6.38. δ ^{29}Si NMR (79 MHz, C_6D_6) -8.95, -35.08, -38.65, -41.63, -109.46. HRMS (EI) m/z: calculated for $C_{14}H_{42}Si_8$ [M-H_2] 434.1441, found 434.1440.

NMR Spectroscopy

^{1}H NMR, ^{13}C NMR, ^{29}Si {^{1}H} DEPT NMR, ^{29}Si INEPT+ NMR, ^{1}H-^{29}Si HSQC NMR, ^{1}H-^{29}Si HMBC NMR, and ^{1}H-^{1}H gCOSY spectra were recorded on a Bruker 400 MHz spectrometer equipped with either a Bruker Avance I or Avance III HD console and chemical shifts are reported in parts per million (ppm). Spectra were recorded in C_6D_6 with tetramethylsilane or the residual solvent peak as the internal standard (^{1}H NMR: C_6H_6 δ = 7.16, ^{13}C NMR: C_6H_6 δ = 128.06). Multiplicities are as indicated: s (singlet), d (doublet), m (multiplet), and br (broad). Coupling constants, *J*, are reported in hertz and integration is provided. All samples of $\mathbf{5}^{2-}$•2[K(18-cr-6)]$^{+}$, $\mathbf{7}^{2-}$•2[K(18-cr-6)]$^{+}$, and **1** were loaded into 5.0 mm Wilmad low pressure/vacuum NMR tubes under nitrogen atmospheres and all samples were kept at standard

temperature and pressure. All NMR spectra were processed using Bruker Topspin 4.0.6 and prepared for publication in Mestrenova 14.1.2.

Standard Bruker pulse programs were applied in all experiments. Specific pulse sequences and relevant parameters are listed below. ^{1}H NMR experiments were performed using the zg30 pulse sequence with a 1 second recycle delay and a 30° pulse flip angle. ^{29}Si {^{1}H} DEPT NMR experiments were performed with the *dept45* pulse sequence using the coupling constant *cnst2* = 7 Hz for J_{SiH}. 128 scans were collected on a 5 second recycle delay with FID size *TD* = 65536 and loop counter *TD0* = 4. ^{29}Si INEPT+ NMR experiments were performed with the *ineptpnd* pulse sequence using the coupling constant *cnst2* = 7 Hz or 120 Hz for J_{SiH}. 128 scans were collected on a 5 second recycle delay with FID size *TD* = 65536 and loop counter *TD0* = 4. ^{1}H-^{29}Si HSQC NMR experiments were performed with the *hsqcedetgp* pulse sequence using the coupling constant *cnst2* = 120 Hz for J_{SiH}. 60 scans were collected on a 1.5 second recycle delay with an FID size of 4096 in *F2* by 512 in *F1* and loop counter *TD0* = 1. ^{1}H-^{29}Si HMBC NMR experiments were performed with the *hmbcgplpndqf* pulse sequence using the coupling constant *cnst2* = 3 Hz, 7Hz, or 10 Hz for J_{SiH}. 56 scans were collected on a 1.5 second recycle delay with an FID size of 4096 in *F2* by 512 in *F1* and loop counter *TD0* = 1. ^{1}H-^{1}H gCOSY NMR experiments were performed with the *cosygpqf* pulse sequence. 12 scans were collected on a 2 second recycle delay with an FID size of 2048 in *F2* by 128 in *F1* and loop counter *TD0* = 1.

Conflicts of interest

There are no conflicts to declare.

Acknowledgements

This research was supported by the U.S. Department of Energy (DOE), Office of Science, Basic Energy Sciences, under Award No. DE-SC0020681.

Notes and references

1 R. D. Miller and J. Michl, *Chem. Rev.*, 1989, **89**, 1359–1410.
2 M. H. Garner, H. Li, M. Neupane, Q. Zou, T. Liu, T. A. Su, Z. Shangguan, D. W. Paley, F. Ng, S. Xiao, C. Nuckolls, L. Venkataraman and G. C. Solomon, *J. Am. Chem. Soc.*, 2019, **141**, 15471–15476.
3 V. Christopoulos, M. Rotzinger, M. Gerwig, J. Seidel, E. Kroke, M. Holthausen, O. Wunnicke, A. Torvisco, R. Fischer, M. Haas and H. Stueger, *Inorg. Chem.*, 2019, **58**, 8820–8828.
4 M. Karplus, *J. Am. Chem. Soc.*, 1963, 85, 2870–2871.
5 M. Barfield and B. Chakrabarti, *Chem. Rev.*, 1969, **69**, 757–778.
6 W. A. Thomas, *Prog. Nucl. Magn. Reson. Spectrosc.*, 1997, **30**, 183–207.
7 R. H. Contreras and J. E. Peralta, *Prog. Nucl. Magn. Reson. Spectrosc.*, 2000, **37**, 321–425.
8 A. Padwa, E. Shefter and E. Alexander, *J. Am. Chem. Soc.*, 1968, **90**, 3717–3721.
9 K. L. Williamson, T. Howell and T. A. Spencer, *J. Am. Chem. Soc.*, 1966, **88**, 325–334.
10 E. A. Marro, C. P. Folster, E. M. Press, H. Im, J. T. Ferguson, M. A. Siegler and R. S. Klausen, *J. Am. Chem. Soc.*, 2019, **141**, 17926–17936.
11 E. L. Eliel, N. L. Allinger, S. J. Angyal and G. A. Morrison, *Conformational Analysis*, Interscience Publishers, Inc., New York, NY, 1981.
12 W. B. Moniz and J. A. Dixon, *J. Am. Chem. Soc.*, 1961, **83**, 1671–1675.
13 C. P. Folster, P. N. Nguyen and R. S. Klausen, *Dalt. Trans.*, 2020, DOI: 10.1039/C9DT04468J.
14 E. M. Press, E. A. Marro, S. K. Surampudi, M. A. Siegler, J. A. Tang and R. S. Klausen, *Angew. Chemie Int. Ed.*, 2017, **56**, 568–572.
15 E. A. Marro, E. M. Press, M. A. Siegler and R. S. Klausen, *J. Am. Chem. Soc.*, 2018, **140**, 5976–5986.
16 C. P. Folster and R. S. Klausen, *Polym. Chem.*, 2018, **9**, 1938–1941.
17 E. A. Marro and R. S. Klausen, *Chem. Mater.*, 2019, **31**, 2202–2211.
18 R. W. Dorn, E. A. Marro, M. P. Hanrahan, R. S. Klausen and A. J. Rossini, *Chem. Mater.*, 2019, **31**, 9168–9178.
19 R. Fischer, T. Konopa, S. Ully, J. Baumgartner and C. Marschner, *J. Organomet. Chem.*, 2003, **685**, 79–92.
20 L. H. Sommer and R. Mason, *J. Am. Chem. Soc.*, 1965, **87**, 1619–1620.
21 V. H. Gessner, C. Däschlein and C. Strohmann, *Chem. - A Eur. J.*, 2009, **15**, 3320–3334.
22 C. Präsang and D. Scheschkewitz, *Struct. Bond.*, 2014, **156**, 1–47.
23 M. Flock and C. Marschner, *Chem. - A Eur. J.*, 2002, **8**, 1024.
24 M. Zirngast, J. Baumgartner and C. Marschner, *Organometallics*, 2008, **27**, 6472–6478.
25 R. S. Klausen, J. R. Widawsky, M. L. Steigerwald, L. Venkataraman and C. Nuckolls, *J. Am. Chem. Soc.*, 2012, **134**, 4541–4544.
26 H. Gilman and G. D. Lichtenwalter, *J. Am. Chem. Soc.*, 1958, **80**, 608–611.
27 H. Gilman and C. L. Smith, *J. Organomet. Chem.*, 1967, **8**, 245–253.
28 R. Fischer, D. Frank, W. Gaderbauer, C. Kayser, C. Mechtler, J. Baumgartner and C. Marschner, *Organometallics*, 2003, **22**, 3723–3731.
29 J. Baumgartner, D. Frank, C. Kayser and C. Marschner, *Organometallics*, 2005, **24**, 750–761.
30 A. Wallner, M. Hölbling, J. Baumgartner and C. Marschner, *Silicon Chem.*, 2007, **3**, 175–185.
31 T. Wiesner, M. Leypold, A. Steinmaurer, D. Schnalzer, R. C. Fischer, A. Torvisco and M. Haas, *Organometallics*, , DOI:10.1021/acs.organomet.0c00385.

32 E. A. Marro, E. M. Press, T. K. Purkait, D. Jimenez, M. A. Siegler and R. S. Klausen, *Chem. - A Eur. J.*, 2017, **23**, 15633–15637.
33 A. Kawachi and K. Tamao, *J. Organomet. Chem.*, 2000, **601**, 259–266.
34 R. R. Gupta and M. D. Lechner, *Chemical Shifts and Coupling Constants for Silicon-29*, 2008, vol. 35F.
35 F. A. Carey and R. J. Sundberg, *Advanced Organic Chemistry, Part A: Structure and Mechanism*, 2007.
36 M. G. Constantino, V. Lacerda, G. V. J. da Silva, L. Tasic and R. Rittner, *J. Mol. Struct.*, 2001, **597**, 129–136.
37 C. P. Butts, C. R. Jones, E. C. Towers, J. L. Flynn, L. Appleby and N. J. Barron, *Org. Biomol. Chem.*, 2011, **9**, 177–184.
38 G. Tekautz, A. Binter, K. Hassler and M. Flock, *ChemPhysChem*, 2006, **7**, 421–429.
39 D. K. Dalling and D. M. Grant, *J. Am. Chem. Soc.*, 1967, **89**, 6612–6622.
40 F. A. L. Anet, C. H. Bradley and G. W. Buchanan, *J. Am. Chem. Soc.*, 1971, **93**, 258–259.
41 H. Booth and J. R. Everett, *J. Chem. Soc. Perkin Trans. 2*, 1980, 255–259.
42 D. Casarini, L. Lunazzi and A. Mazzanti, *Tetrahedron*, 1998, **54**, 13181–13184.
43 M. H. Garner, H. Li, Y. Chen, T. A. Su, Z. Shangguan, D. W. Paley, T. Liu, F. Ng, H. Li, S. Xiao, C. Nuckolls, L. Venkataraman and G. C. Solomon, *Nature*, 2018, **558**, 415–419.
44 T. K. Purkait, E. M. Press, E. A. Marro, M. A. Siegler and R. S. Klausen, *Organometallics*, 2019, **38**, 1688–1698.
45 Y. Heider, P. Willmes, V. Huch, M. Zimmer and D. Scheschkewitz, *J. Am. Chem. Soc.*, 2019, **141**, 19498–19504.
46 M. Haas, A. Knoechl, T. Wiesner, A. Torvisco, R. Fischer and C. Jones, *Organometallics*, 2019, **38**, 4158–4170.

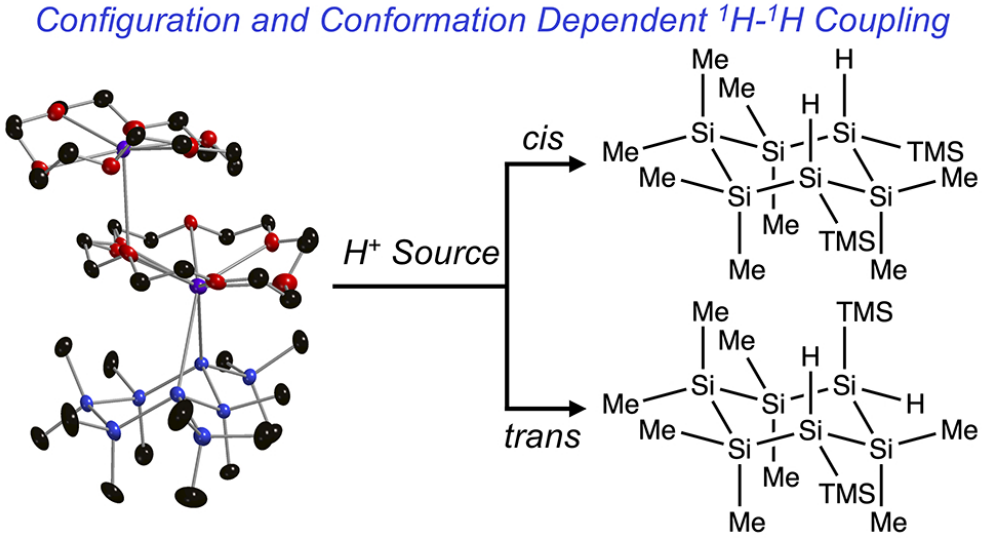

82x45mm (300 x 300 DPI)